

# Supplementary Materials

## Supplementary Material to Section 3.1. Characteristics of PS Beads

The synthesis of PS particles as described in Section 2.2 enables tuning of the surface charge of the desired beads. According to the reaction mechanism of the radical emulsion polymerization the initiator molecules form radical species which attack the small amount of styrene monomer dissolved in water. Oligomers are formed due to chain propagation reaction and finally start to precipitate. Then, the precipitated hydrophobic polymer chains form a spherical shape to minimize their interface with the surrounding aqueous media. While this happens the charged and hydrophilic groups of every polymer chain, originating from the initiator molecule as shown in Figure S1, assemble at the outer surface of the polystyrene bead to result in a highly charged particle surface. After this first nucleation process particle growth continues by addition of more precipitating oligomer and polymer chains. The particle formation of uncharged PS beads follows a similar mechanism, where the start and buildup of oligomers takes place inside of the dispersed styrene droplets, which then precipitate in aqueous solution forming spherical beads.

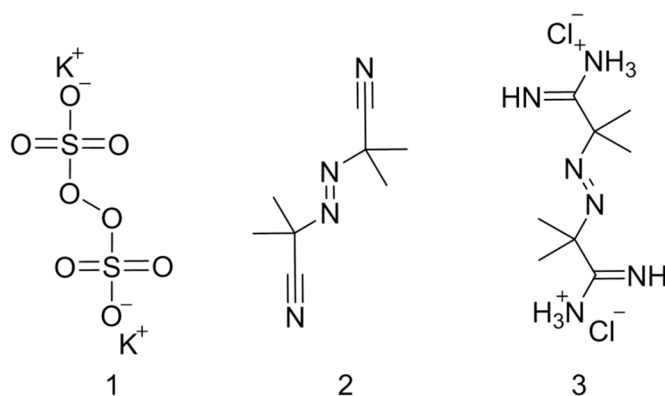


Figure S1. Initiator molecules (1) KPS; (2) AIBN; (3) AIBA.

The particle growth depends on many different parameters: choice of initiator and surfactant, reaction time, concentration of styrene, initiator and surfactant, impeller shape and speed, temperature and delay time before addition of surfactant. Because this study is focused on using these particles for membrane fouling we just varied the reaction time to adjust the particle size to a value of around 0.2  $\mu\text{m}$ , which is smaller than the pore size of the PVDF membrane (0.45  $\mu\text{m}$ ). Therefore, particles can pass through the membrane when no interactions between membrane and particles occur, and fouling due to size exclusion is prevented. The polydispersity index (PDI) characterizes the degree of polydispersity of the particle sizes. Particle suspensions with a PDI below 0.05 can be assumed to be monodisperse, which applies to all synthesized particle suspensions (Figure S2a). The particle diameters (Figure S2a) were determined with dynamic light scattering and have been confirmed by SEM pictures taken from particles, which were spincoated on silica wafers as shown in Figure S2b for cationic PS beads.

a	beads	particle diameter [nm]	PDI	b
	anionic	183	0.015	
	uncharged	211	0.013	
	cationic	220	0.018	

Figure S2. (a) Particle size and PDI of PS beads; (b) SEM picture of cationic PS beads.

### Supplementary Material to Section 3.2. Characteristics of Modified PVDF Membranes

The modification of PVDF membranes as described in section 2.3 with the reagents shown in Figure 2 enables to permanently hydrophilize a membrane's surface. Due to the electron beam irradiation radical species are formed, which lead, following a grafting reaction, to a chemical bonding between the membrane and the used modification reagent.

In the case of the PVDF-TEPA membrane aminoethyl methacrylate (AEMA, Figure 2.1) is grafted on the membrane surface following a grafting-from mechanism leading to polymer chain growth, which starts at the membrane surface and builds up polymer chains containing amino functions. These functions will then be used to react with glutaraldehyde (Figure 2.1) forming a Schiff base. The remaining aldehyde function forms in a subsequent reaction, again, a Schiff base with the amino groups of TEPA (Figure 2.1) to give an alkaline structure (Figure S3.1). To obtain the alkaline structure of the PVDF-TEPA membrane (Figure S3.2) the reactions with GA and TEPA are repeated to further improve the density of functional groups.

The reaction with either PEG (Figure 2.2) or PSS (Figure 2.3) follows a grafting-to mechanism leading to the formation of either PVDF-PEG or PVDF-PSS membranes. Here, no further chemical reactions are needed to gain the final membrane modification.

To obtain the PVDF-Lysine membrane a grafting-from reaction with AEMA (Figure 2.4) and the subsequent reaction with GA (Figure 2.4) are conducted as described for the PVDF-TEPA membrane. Then, the remaining aldehyde function forms a Schiff base with the amino group of lysine (Figure 2.4) resulting in the zwitterionic structure of the PVDF-Lysine membrane (Figure S3.3).

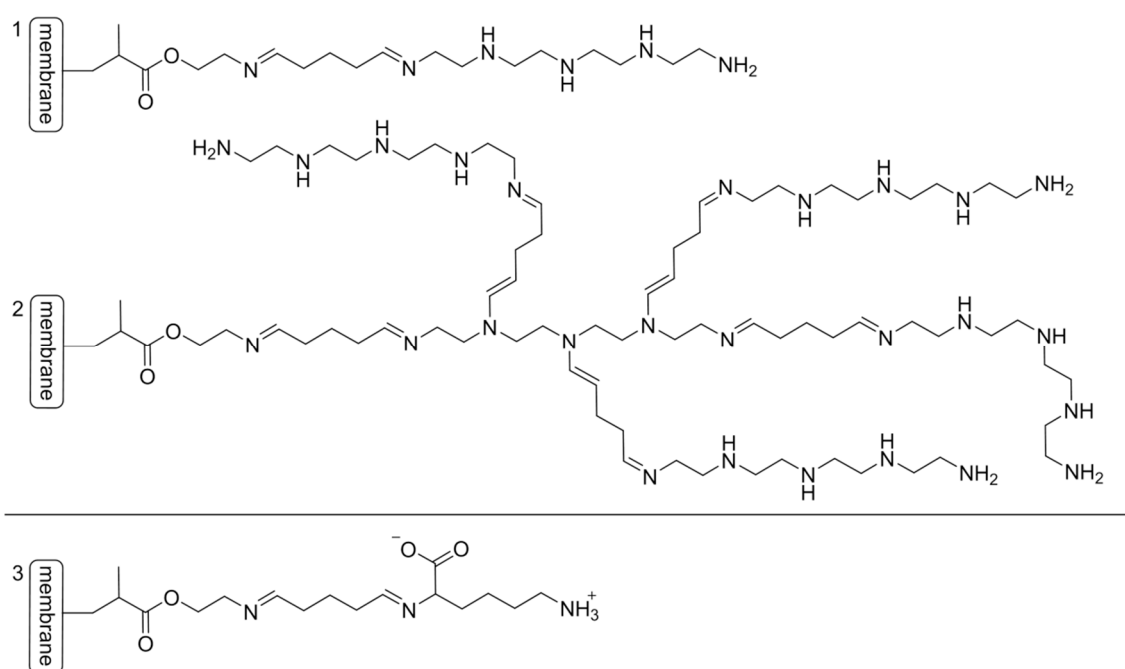


**Figure S3.** Structures of modifications (1) PVDF-TEPA (intermediate), (2) PVDF-TEPA, (3) PVDF-Lysine.

The morphology of the different modified membranes was investigated using SEM and mercury porosimetry. SEM pictures of the untreated and modified membrane's top side are shown in Figure S4. The open pore structure remains without unwanted pore blocking independent of the applied modification. This is in agreement with the results obtained from mercury porosimetry, which are shown in Table S1. All samples have a porosity of around 70% and an average pore size of 0.90  $\mu\text{m}$  proving that no pore blocking occurred due to the membrane modification. The difference in pore size between the gained data and the pore size given by the manufacturer (0.45  $\mu\text{m}$ ) can be explained by different pore characterization methods. The water permeation flux also remained the same for all membranes and was determined to be about 30–36 mL/(min  $\text{cm}^2$  bar).

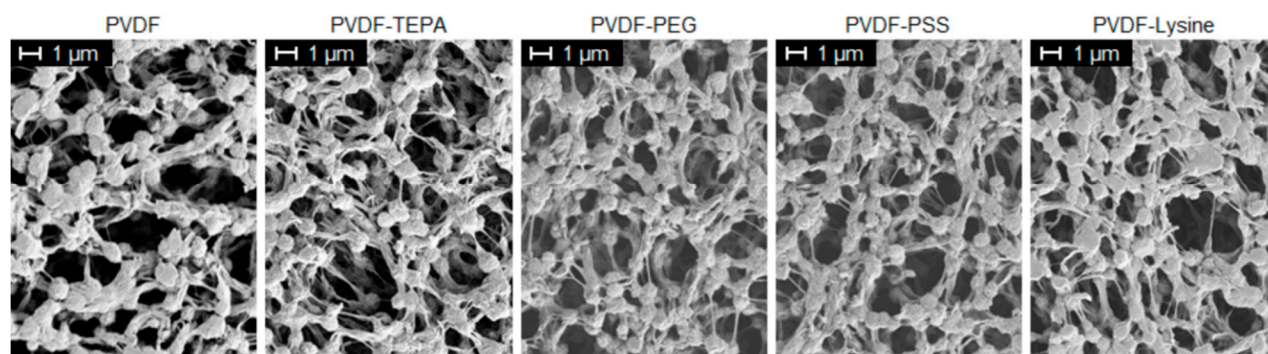


Figure S4. SEM pictures of top side of modified membranes.

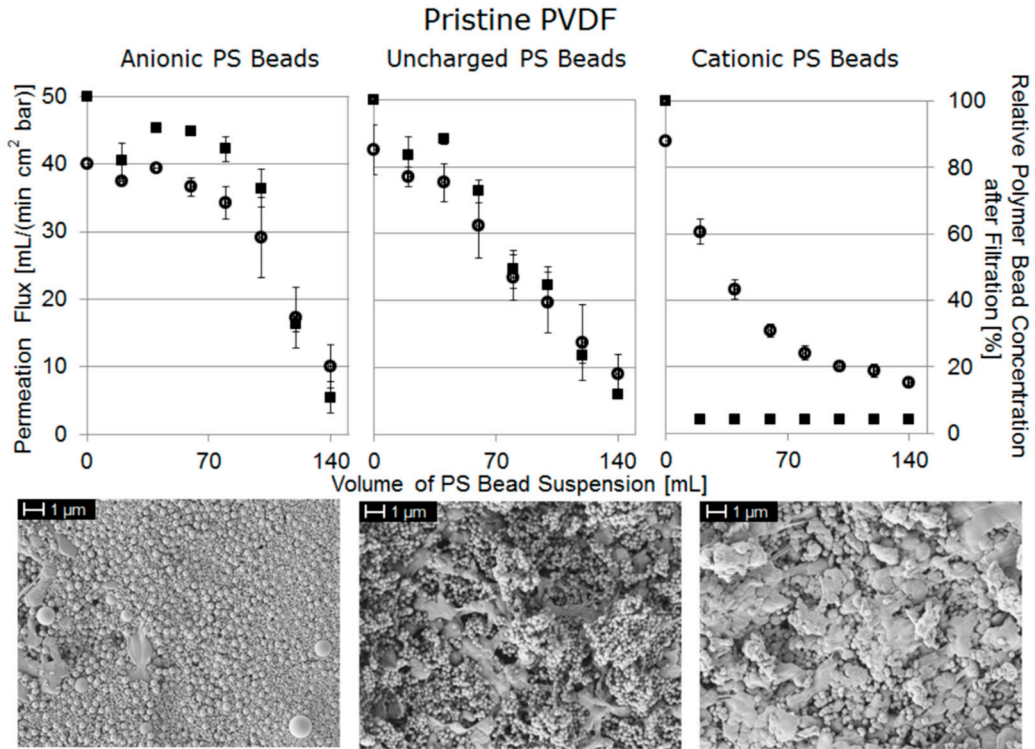
XPS elemental composition also varies for the differently modified membranes. While the pure PVDF membrane is just composed of carbon and fluorine PVDF-TEPA shows significant values of oxygen (8.5%) and nitrogen (3.9%) resulting from the applied alkaline dendrimeric structure. PEG and PSS modifications result in membrane surfaces including a higher amount of oxygen (PVDF-PEG: 6.1% and PVDF-PSS: 2.1%) and in the case of PVDF-PSS also sulfur (0.2%) is present. For the zwitterionic PVDF-Lysine membrane both nitrogen (1.0%) and oxygen (6.4%) quantities are increased representing the grafted structure shown in Figure S3.3. Detailed information on XPS data are presented in Table S1, chemical structures of the different modification reagents are shown in Figure 2 and the resulting structures of PVDF-TEPA and -Lysine as well as an intermediate structure of PVDF-TEPA can be seen in Figure S3.

Table S1 Characteristics of modified PVDF membranes.

	PVDF	PVDF-TEPA	PVDF-PEG	PVDF-PSS	PVDF-Lysine	
water permeation flux [mL/(min cm <sup>2</sup> bar)]	33.7 ± 1.6	30.8 ± 0.9	34.5 ± 2.1	36.3 ± 1.5	30.0 ± 1.8	
Porosity [%]	72 ± 2	72 ± 2	72 ± 6	69 ± 1	72 ± 2	
Average pore size [μm]	0.9 ± 0.04	1.0 ± 0.09	0.9 ± 0.04	0.9 ± 0.05	0.9 ± 0.03	
Elemental composition [%]	C	51.8	53.8	49.3	45.2	50.3
	O	0.2	8.5	8.9	2.1	6.4
	N	-	3.9	-	-	1.0
	F	48.0	33.8	41.8	52.5	42.3
	S	-	-	-	0.2	-

### Supplementary Material to Section 3.3. Membrane Fouling with PS Beads

The following Figures S5–S9 show the complete overview of fouling characteristics of the different membranes towards anionic, uncharged, and cationic PS beads. Permeation flux and the relative concentration of polymer beads in the filtrate are plotted against the volume of PS bead suspension passed through the membrane. The corresponding SEM pictures of the different membranes after fouling are shown below every particular diagram.



**Figure S5.** Permeation flux of fouling suspension (left axis, open circles) and normalized concentration of PS beads in filtrate (right axis, filled squares) *vs.* volume of PS bead suspension, and corresponding SEM pictures of the pristine PVDF membrane after fouling.

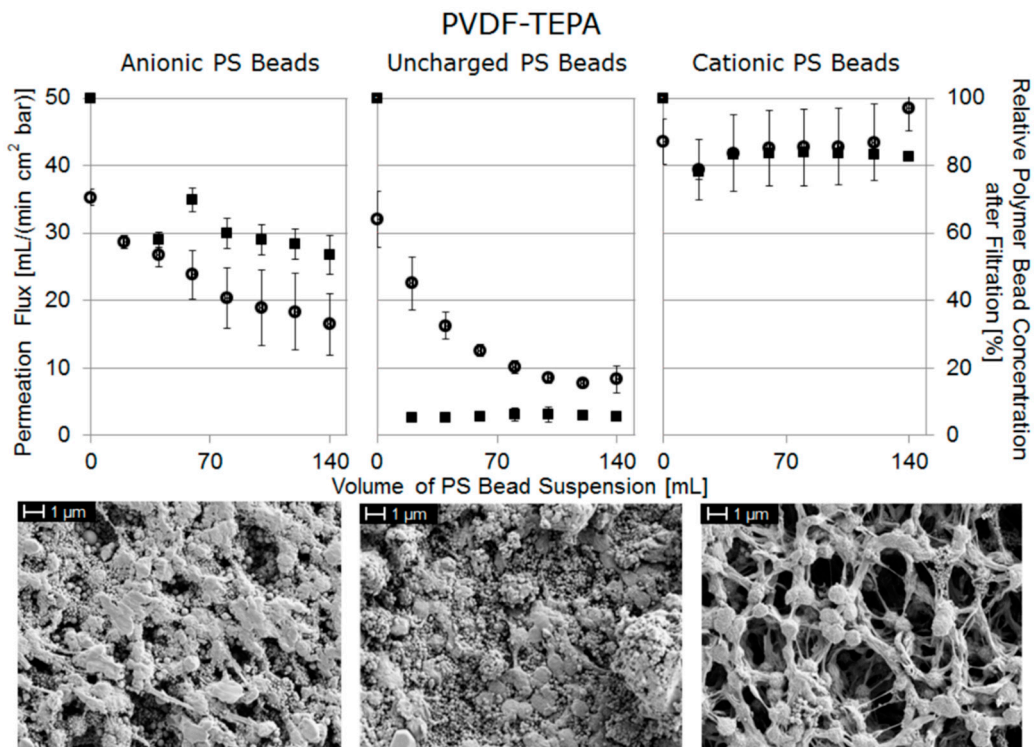


**Figure S6.** Permeation flux of fouling suspension (left axis, open circles) and normalized concentration of PS beads in filtrate (right axis, filled squares) *vs.* volume of PS bead suspension, and corresponding SEM pictures of the PVDF-TEPA membrane after fouling.

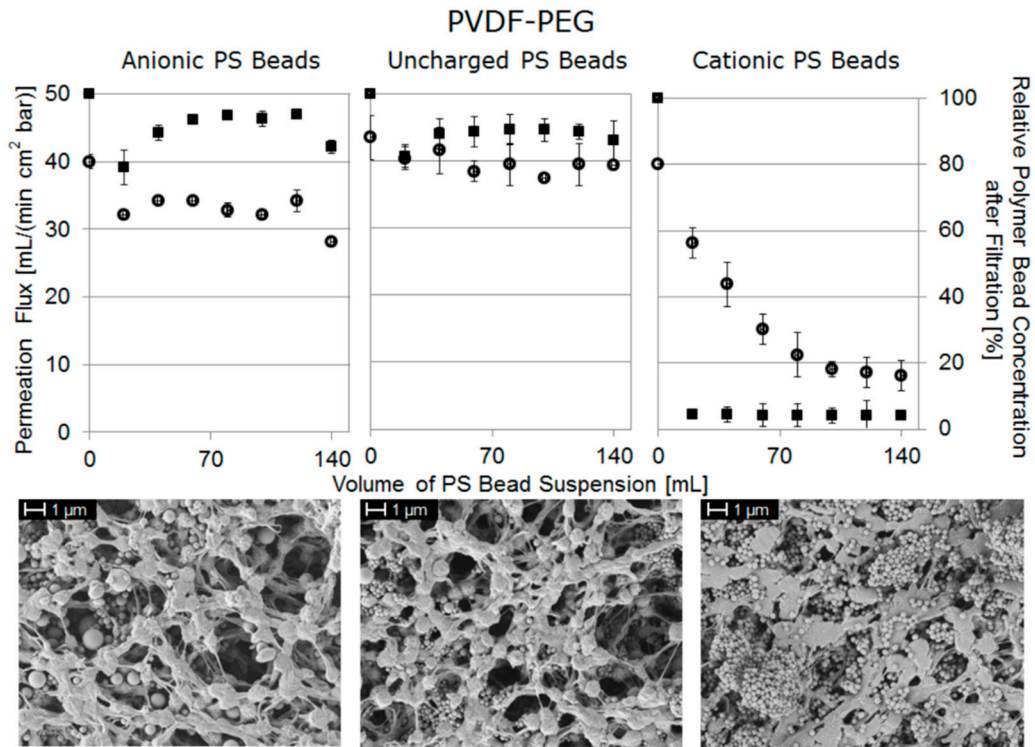


**Figure S7.** Permeation flux of fouling suspension (left axis, open circles) and normalized concentration of PS beads in filtrate (right axis, filled squares) *vs.* volume of PS bead suspension, and corresponding SEM pictures of the PVDF-PEG membrane after fouling.

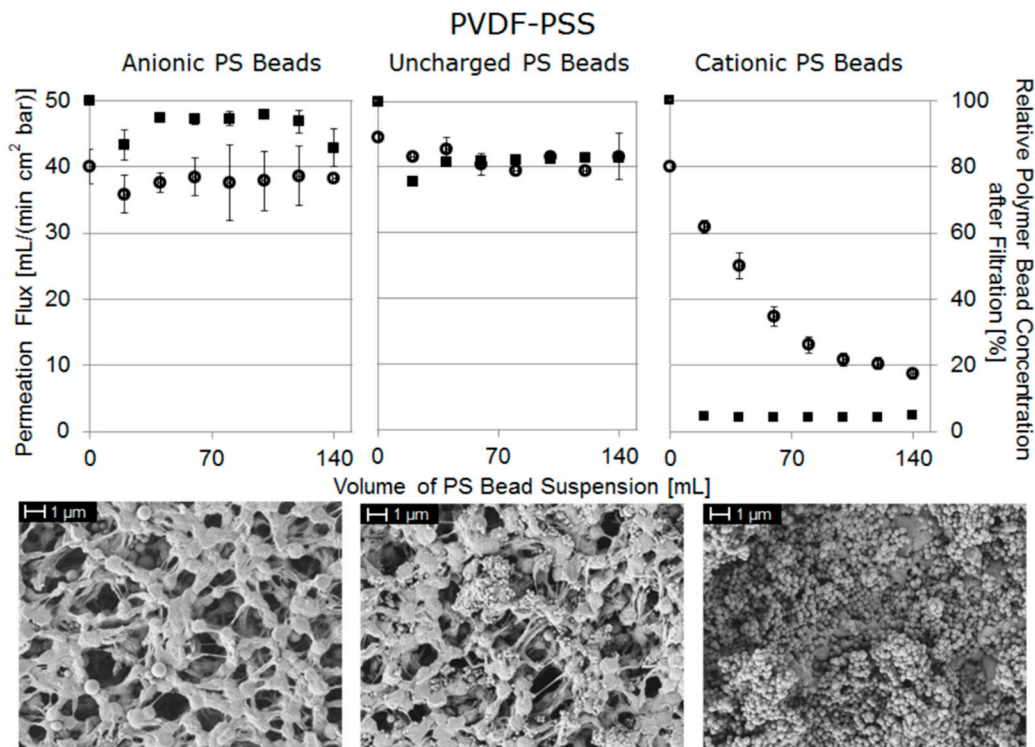


**Figure S8.** Permeation flux of fouling suspension (left axis, open circles) and normalized concentration of PS beads in filtrate (right axis, filled squares) *vs.* volume of PS bead suspension, and corresponding SEM pictures of the PVDF-PSS membrane after fouling.

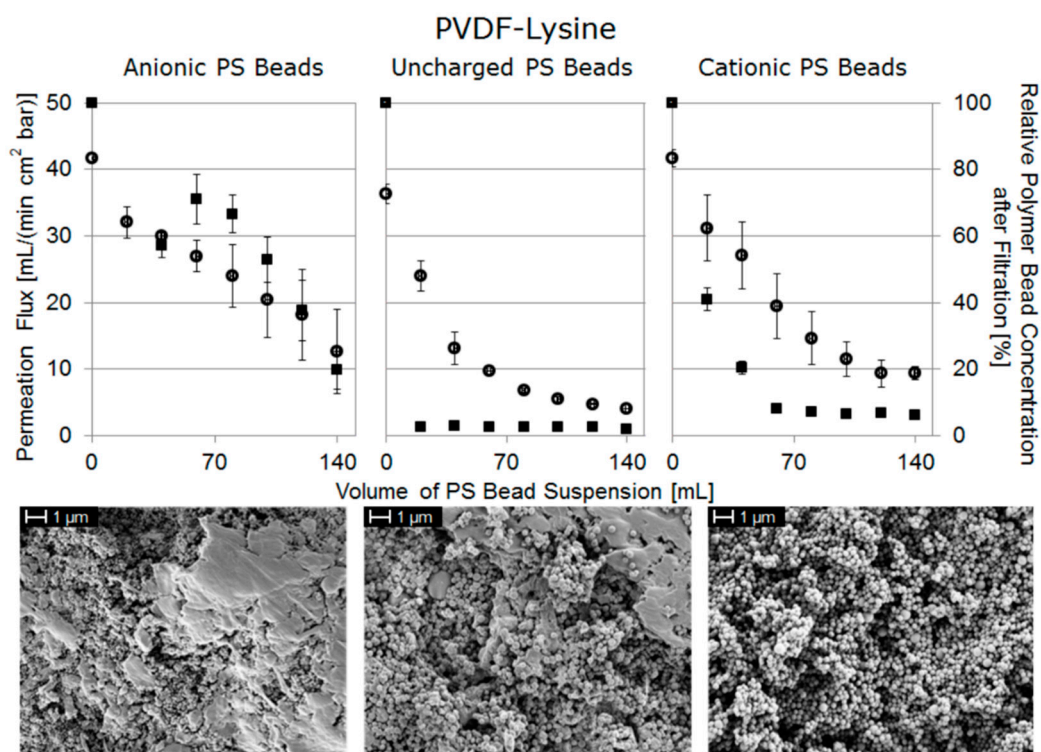


**Figure S9.** Permeation flux of fouling suspension (left axis, open circles) and normalized concentration of PS beads in filtrate (right axis, filled squares) *vs.* volume of PS bead suspension, and corresponding SEM pictures of the PVDF-Lysine membrane after fouling.



© 2015 by the authors; licensee MDPI, Basel, Switzerland. This article is an open access article distributed under the terms and conditions of the Creative Commons by Attribution (CC-BY) license (<http://creativecommons.org/licenses/by/4.0/>).